ISSN (Print) 1226-1750
ISSN (Online) 2233-6656
Journal of Magnetics 24(2), 202-211 (2019) https://doi.org/10.4283/JMAG.2019.24.2.202

Melting Heat Transfer in Thermally Stratified Magnetohydrodynamic Flow of Eyring-Powell Fluid with Homogeneous-heterogeneous Reaction

M. Javed*, M. Farooq, S. Ahmad, and Aisha Anjum

Department of Mathematics, Riphah International University, Islamabad 44000, Pakistan

(Received 18 June 2018, Received in final form 5 March 2019, Accepted 4 April 2019)

Features of melting heat transfer as well as homogeneous-heterogeneous reaction in thermally stratified stagnation flow of Eyring-Powell fluid along with heat generation/absorption effects are explored in this article. Fluid flow is examined over a sheet of variable thickness in the presence of stretching phenomena. Variable strength of magnetic field is considered normal to the flow field. Suitable transformations are introduced for the sake of conversion of partial differential equations to ordinary differential equations. Homotopic method is utilized to tackle highly nonlinear problem and series solutions are attained. Behaviors of relevant parameters are portrayed for velocity, thermal and concentration distributions. Graphical results reveal that the concentration profile enhances for higher Schmidt number while it exhibits recessive behavior for increment in homogeneous reaction parameter. Larger values of heterogeneous reaction parameter result in intensified concentration field. Velocity field declines as a result of increment in fluid parameters ε as well as δ^*.

Keywords : Melting heat transfer, MHD, Eyring-Powell fluid, Homogeneous-heterogeneous reaction, Heat generation/absorption, Stagnation point, Variable sheet thickness

Nomenclature

α_1 : Thermal conductivity
u, v : Velocity components
T : Fluid temperature
T_m : Melting surface temperature
B : Magnetic field
S : Thermal stratification
U_w : Stretching velocity
U_e : Ambient velocity
Re : Reynolds number
Sc : Schmidt number
Ha : Hartmann number
A : Ratio of velocity
C_f : Skin friction coefficient
Nu : Nusselt number
M : Melting parameter
Pr : Prandtl number
λ_1 : Latent Heat
T_∞ : Free stream temperature
K : Homogeneous reaction parameter
K_s : Heterogeneous reaction parameter
c_p : Specific heat capacity
B_0 : Applied magnetic field
k : Thermal conductivity
ν : Kinematic viscosity
δ : Ratio of mass diffusion coefficients
ρ : Fluid density
η, ξ : Similarity variable
θ : Dimensionless temperature
μ : Dynamic viscosity
τ_{xy} : Shear stresses
λ : Heat generation/absorption parameter
σ : Dimensionless reaction rate
ε, δ^* : Material fluid parameters
σ : Electric conductivity
α : Wall thickness parameter

1. Introduction

There are abundant chemically reacting processes which involve heterogeneous and homogeneous reactions. Several complicated relations are involved in these type of reactions. Amongst all, fewer reactions of them are totally unable to proceed or have low capacity in this regard except for case in presence of catalyst. Such types

*Corresponding author: Tel: +92-300-5301637
Fax: +92-323-5248918, e-mail: mubashar.bstar@yahoo.com

of reactions occur in biochemical systems, fog formation as well as dispersion, hydrometallurgical industry, processing of foods, production of polymer and ceramics etc. Merkin [1] suggested an isothermal model to study viscous fluid flow along with chemical species. Yasmeen *et al*. [2] investigated features of chemical species in Ferrofluid flow. Sandeep *et al.* [3] analyzed the Jeffrey Nanofluid flow along with chemical reactions and induced magnetic field. Khan *et al.* [4] focused on chemical species analysis for Casson fluid flow. An exclusive analysis for the flow of carbon nanotubes with chemical species is given by Hayat *et al.* [5]. Lu *et al.* [6] interrogated the interactive relation of heterogeneous-homogeneous reaction of air and hydrogen mixture.

Analysis of fluid flow along with heat transfer because of stretched surface has tremendous utilization in polymer industries and plenty of production processes. Heat transfer via melting process is extensively involved in the modern industrial and technological processes due to which numerous researchers are keen to explore it. Its industrial applications include melting of permafrost and thawing of frozen grounds, magma solidification, glass blowing, portrayal of plastic films and fibre technology. Adegbie *et al.* [7] scrutinized the heat transfer impact via melting process for the flow of micropolar fluid. Mahmoud and Waheed [8] addressed the aspects of heat transfer through micropolar fluid along with phenomenon of melting. Influence of melting heat transfer for magnetohydrodynamic flow is described by Abel and Sanamani [9]. Mabood and Das [10] made an effort to discuss the melting heat phenomenon of nanofluid flow along with radiative effects and slip condition of second order. Heat transfer by melting phenomena with dual stratification effects in viscous nanofluid flow are elaborated by Farooq *et al.* [11]. Javed *et al.* [12] communicated process of melting heat transfer in thermally stratified flow entrenched in porous medium along with radiative effects.

Behaviors of non-Newtonian fluid flows [13-25] have attracted researchers because of their significant applications in chemical and petroleum industries, metallurgical processes, fibre technology, food products, biological sciences and so forth. Several constitutive relations have been proposed in literature to construe non-Newtonian materials. Such materials can be divided in to three categories integral, differential and rate type fluids. Several years ago in 1944, Eyring and Powell [26] presented Eyring-Powell fluid model. In order to derive this model, kinetic theory of gases has been utilized instead of the empirical relation. Eyring-Powell fluids have the ability to recover Newtonian behavior at high and low shear rates. Tooth paste, ketchup and blood are some of examples representing Eyring-Powell fluid. Such fluid flow over stretched sheet with thermal conductivity of variable nature is reported by Megahed [27]. Jalil *et al.* [28] discussed the properties of heat transfer of Eyring-Powell fluid on a moving surface. Ara *et al.* [29] analyzed thermal radiative impact on Eyring-Powell fluid towards a sheet which is exponentially shrinking. A comparative study of Eyring-Powell fluid with heat generation/absorption effects is carried out by Hayat *et al.* [30]. Some relevant studies can be found in [31-33].

Our aim here is to reconnoiter melting heat transfer aspects along with chemical species in Eyring-Powell fluid flow over a sheet of variable thickness. To disclose features of fluid flow, nonlinear stretching phenomena is employed. Heat generation/absorption effects are also considered in this study. Further stagnation point is retained here. Suitable transformations are utilized to transmute nonlinear PDE's to nonlinear ODE's which are then tackled by the method of Homotopic analysis *HAM* [37-46] to attain series solution. Graphical behaviors of relevant parameters are portrayed for velocity, thermal and concentration distributions.

2. Mathematical Formulation

We consider a plate possessing variable thickness over which stagnation flow of Eyring-Powell fluid is examined. Features of heat transfer are explored by making use of more appropriate condition (melting heat transfer) on surface. Homogeneous-heterogeneous reaction as well as heat generation/absorption effects are also deliberated here. Varying magnetic field is operated normal to flow field. Ambient temperature T_∞ is dominant as compared to the wall temperature T_m.

Further we have taken similar diffusion coefficients for both species. Advanced model regarding homogeneous-heterogeneous reaction is carefully selected as [1]:

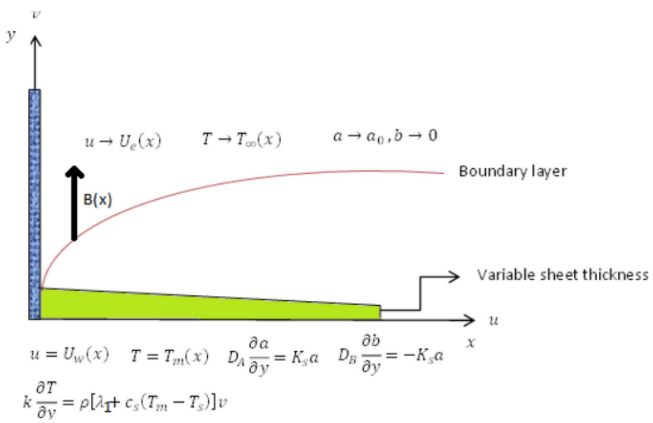

Fig. 1. (Color online) Geometry of problem.

$A+2B\to 3B,\quad rate=k_c ab^2,$

The catalytic 1st order isothermal reaction is designated by

$A+B\to 3B,\quad rate=k_s a.$

Here a and b signify the concerning concentrations of chemical species A and B. While k_c and k_s represent rate constants. By making use of boundary layer approximations, flow analysis under consideration become:

$$\frac{\partial u}{\partial x}+\frac{\partial v}{\partial y}=0, \tag{1}$$

$$u\frac{\partial u}{\partial x}+v\frac{\partial u}{\partial y}=U_e\frac{dU_e}{dx}+\left(\nu+\frac{1}{\rho\beta C_1}\right)\frac{\partial^2 u}{\partial y^2} -\frac{1}{2\rho\beta C_1^3}\left(\frac{\partial u}{\partial y}\right)^2\frac{\partial^2 u}{\partial y^2}-\frac{\sigma B^2(x)}{\rho}(u-U_e), \tag{2}$$

$$u\frac{\partial T}{\partial x}+v\frac{\partial T}{\partial y}=\alpha_1\frac{\partial^2 T}{\partial y^2}+\frac{Q_0}{\rho c_p}(T-T_m), \tag{3}$$

$$u\frac{\partial a}{\partial x}+v\frac{\partial a}{\partial y}=D_A\frac{\partial^2 a}{\partial y^2}-K_1 ab^2, \tag{4}$$

$$u\frac{\partial b}{\partial x}+v\frac{\partial b}{\partial y}=D_B\frac{\partial^2 b}{\partial y^2}+K_1 ab^2, \tag{5}$$

along relevant conditions at boundary,

$$u=U_w(x)=U_0(x+b_1)^n,\ T=T_m(x)=T_0+c(x+b_1),$$
$$D_A\frac{\partial a}{\partial y}=K_s a\ \ D_B\frac{\partial b}{\partial y}=-K_s a\ \ \text{at } y=B^*(x+b_1)^{\frac{1-n}{2}},$$
$$k\left(\frac{\partial T}{\partial y}\right)_{B^*(x+b_1)^{\frac{1-n}{2}}}=\rho[\lambda_1+c_s(T_m-T_0)]v_{B^*(x+b_1)^{\frac{1-n}{2}}}, \tag{6}$$
$$u\to U_e(x)=U_\infty(x+b_1)^n,\ T=T_\infty(x)=T_0+d(x+b_1),$$
$$a\to a_0,\ \ b\to 0\ \text{ when }\ y\to\infty.$$

In x and y directions we have represented the velocity components by u and v respectively, stretching velocity by U_w, ambient velocity by U_e, kinematic viscosity by ν, power index by n, a_0, B^*, c and d are dimensional constants, c_s denote specific heat of solid surface, ρ stands for density, λ_1 signifies latent heat, D_A and D_B show diffusion coefficients for species A and B respectively, T and T_m express fluid temperature and melting surface temperature respectively, K_s represent heterogeneous reaction parameter, k the thermal conductivity, T_∞ the free stream temperature, U_0, U_∞ are the velocities for reference and T_0 is reference temperature.

Writing,

$$\psi=\sqrt{\frac{2}{n+1}\nu U_0(x+b_1)^{n+1}}F(\xi),\ \xi=\sqrt{\frac{n+1}{2}\frac{U_0}{\nu}(x+b_1)^{n-1}}y,$$
$$u=U_0(x+b_1)^n F'(\xi),$$
$$v=-\sqrt{\frac{n+1}{2}\nu U_0(x+b_1)^{n-1}}\left(F(\xi)+\xi\frac{n-1}{n+1}F'(\xi)\right), \tag{7}$$
$$\Theta(\xi)=\frac{T-T_m}{T_\infty-T_0},\ G(\xi)=\frac{a}{a_0},\ H(\xi)=\frac{b}{a_0}.$$

the incompressibility condition (Eq. 1) is satisfied automatically , however Eqs. (2-5) become,

$$F'''+\frac{\varepsilon}{1+\varepsilon}FF''-\frac{1+n}{1+\varepsilon}\delta^*(F'')^2F'''+\frac{2n}{1+n}\frac{\varepsilon}{1+\varepsilon} (A^2-(F')^2)+\frac{2Ha}{1+n}\frac{\varepsilon}{1+\varepsilon}(A-F')=0, \tag{8}$$

$$\Theta''-\frac{2\,\mathrm{Pr}}{1+n}\Theta F'-\frac{2\,\mathrm{Pr}}{1+n}SF'+\mathrm{Pr}\,\Theta' F+\frac{2\,\mathrm{Pr}}{1+n}\lambda\theta=0, \tag{9}$$

$$G''-\frac{2ScK}{1+n}GH^2+ScFG'=0, \tag{10}$$

$$H''-\frac{2ScK}{\delta(1+n)}GH^2+\frac{Sc}{\delta}FH'=0, \tag{11}$$

with subjected boundary conditions,

$$F'(\alpha)=1,\ \ F'(\infty)=A,$$
$$M\Theta'(\alpha)+\mathrm{Pr}\left(F(\alpha)+\alpha\frac{n-1}{n+1}\right)=0,$$
$$\Theta(\alpha)=0,\ \ \Theta(\infty)=1-S,$$
$$G'(\alpha)=\sqrt{\frac{2}{n+1}}K_s G(\alpha),\ \ G(\infty)=1, \tag{12}$$
$$H'(\alpha)=-\frac{1}{\delta}\sqrt{\frac{2}{n+1}}K_s G(\alpha),\ \ H(\infty)=0,$$

here $\alpha=B^*\sqrt{\frac{n+1}{2}\frac{U_0}{\nu}}$, while prime denote differentiation with respect to 'ξ'. Letting $F(\xi)=f(\xi-\alpha)=f(\eta)$, $\Theta(\xi)=\theta(\xi-\alpha)=\theta(\eta)$, $G(\xi)=g(\xi-\alpha)=g(\eta)$ and $H(\xi)=h(\xi-\alpha)=h(\eta)$, we have

$$f'''+\frac{\varepsilon}{1+\varepsilon}ff''-\frac{1+n}{1+\varepsilon}\delta^*(f'')^2f'''+\frac{2n}{1+n}\frac{\varepsilon}{1+\varepsilon} (A^2-(f')^2)+\frac{2Ha}{1+n}\frac{\varepsilon}{1+\varepsilon}(A-f')=0, \tag{13}$$

$$\theta''-\frac{2\,\mathrm{Pr}}{1+n}\theta f'-\frac{2\,\mathrm{Pr}}{1+n}Sf'+\mathrm{Pr}\,\theta' f+\frac{2\,\mathrm{Pr}}{1+n}\lambda\theta=0, \tag{14}$$

$$g''-\frac{2ScK}{1+n}gh^2+Scfg'=0, \tag{15}$$

$$h''-\frac{2ScK}{\delta(1+n)}gh^2+\frac{Sc}{\delta}fh'=0, \tag{16}$$

$$M\theta'(0)+\Pr\left(f(0)+\alpha\frac{n-1}{n+1}\right)=0,\ f'(0)=1,\ f'(\infty)=A,$$

$$\theta(0)=0,\quad \theta(\infty)=1-S,$$

$$g'(0)=\sqrt{\frac{2}{n+1}}K_s g(0),\quad g(\infty)=1,$$

$$h'(0)=-\frac{1}{\delta}\sqrt{\frac{2}{n+1}}K_s g(0),\ \ h(\infty)=0. \tag{17}$$

Here Pr denotes the Prandtl number, δ shows ratio of mass diffusion coefficients, δ^* and ε depict material fluid parameters, *Sc* represents Schmidt number, λ denote heat generation/absorption parameter, *K* stands for homogeneous reaction parameter, K_s depicts heterogeneous reaction parameter, *A* is ratio of velocities, *S* signifies thermal stratification, *Ha* the Hartman number, α represents the wall thickness parameter and *M* is melting parameter. Mathematical interpretation for all of these quantities is given below,

$$\Pr=\frac{\mu_f c_p}{k},\ \delta=\frac{D_B}{D_A},\ \delta^*=\frac{U_0(x+b_1)^{3n-1}}{4C_1^2\nu},$$

$$\varepsilon=\mu\beta C_1,\ \lambda=\frac{Q_0(x+b_1)^{1-n}}{\rho c_p U_0},\ Sc=\frac{\nu}{D_A},\ K=\frac{K_1 a_0^2(x+b_1)}{U_w},$$

$$K_s=\frac{k_s}{D_A}\sqrt{\frac{\nu(x+b_1)}{U_w}},\ A=\frac{U_\infty}{U_0},\ S=\frac{c}{d},\ Ha=\frac{\sigma B_0^2}{\rho U_0},$$

$$\alpha=B^*\sqrt{\frac{n+1}{2}\frac{U_0}{\nu}},\ M=\frac{c_p(T_\infty-T_m)}{\lambda_1+c_s(T_m-T_0)}. \tag{18}$$

Here it is important to mention that *M* is combined of Stefan numbers $\frac{c_p(T_\infty-T_m)}{\lambda_1}$ and $\frac{c_s(T_m-T_0)}{\lambda_1}$ of liquid and solid phases respectively. $M=0$ interprets absence of melting phenomena. Similar size of relevant diffusive coefficients of chemical species A and B is presumed. Using this argument we take up equal values of D_A and D_B i.e., $\delta=1$ [5]. Thus,

$$g(\eta)+h(\eta)=1. \tag{19}$$

From Eq. (15-16), we obtain,

$$g''-\frac{2ScK}{n+1}g(1-g)^2+Scfg'=0 \tag{20}$$

$$g'(0)=\sqrt{\frac{2}{n+1}}K_s g(0),\ \ g(\infty)\to 1\ \text{ when }\eta\to\infty. \tag{21}$$

Interpretation for C_f (skin friction coefficient) and *Nu* (Nusselt number) in mathematical form implies,

$$C_f=\frac{\tau_w}{\rho U_w^2},\ \ Nu=\frac{(x+b_1)q_w}{k(T_\infty-T_m)},$$

here mathematical expression for shear stress τ_w as well as heat flux q_w on wall gives,

$$\tau_w=\mu\left(\frac{\partial u}{\partial y}\right)_{y=B^*(x+b_1)^{\frac{1-n}{2}}},\quad q_w=-k\left(\frac{\partial T}{\partial y}\right)_{y=B^*(x+b_1)^{\frac{1-n}{2}}}.$$

Non dimensional form of these quantities is given below,

$$\begin{aligned}&\mathrm{Re}_x^{1/2}C_f=(1+\varepsilon)\sqrt{\frac{n+1}{2}}f''(0)-\frac{\varepsilon}{3}\delta^* f'''(0),\\ &\mathrm{Re}_x^{-1/2}Nu_x=-(1-S)\sqrt{\frac{n+1}{2}}\theta'(0),\end{aligned} \tag{22}$$

Local Reynolds number = $\mathrm{Re}_x=\frac{U_w(x+b_1)}{\nu}$.

3. Homotopic Procedure

Homotopic analysis method (*HAM*) was introduced by Liao [38]. Main target of this method is to counter problems of highly nonlinear nature. It efficiently provides space to pick initial guesses as well as linear operators. Relevant auxiliary operators (linear) and initial approximations for the problem under consideration are selected as follows,

$$f_0(\eta)=A\eta+(1-A)(1-\exp(-\eta))-\left(\frac{(1-S)M}{\Pr}+\alpha\frac{n-1}{n+1}\right), \tag{23}$$

$$\theta_0(\eta)=(1-S)\left(1-\exp(-\eta)\right), \tag{24}$$

$$g_0(\eta)=1-\frac{1}{2}\exp(-\sqrt{\frac{2}{n+1}}K_s\eta), \tag{25}$$

$$\mathbf{L}_f(f)=\frac{d^3f}{d\eta^3}-\frac{df}{d\eta},\ \mathbf{L}_\theta(\theta)=\frac{d^2\theta}{d\eta^2}-\theta,\ \mathbf{L}_g(\theta)=\frac{d^2g}{d\eta^2}-g. \tag{26}$$

The auxiliary linear operators satisfy the below listed operators,

$$\mathbf{L}_f\left[E_1+E_2\exp(\eta)+E_3\exp(-\eta)\right]=0, \tag{27}$$

$$\mathbf{L}_\theta\left[E_4\exp(\eta)+E_5\exp(-\eta)\right]=0, \tag{28}$$

$$\mathbf{L}_g\left[E_6\exp(\eta)+E_7\exp(-\eta)\right]=0, \tag{29}$$

E_i represents arbitrary constants, i = 1, 2,..., 7.

3.1. Deformation of zeroth order

$$(1-q_1^*)\mathbf{L}_f\left[\widehat{f}(\eta;q_1^*)-f_0(\eta)\right]=q_1^*\hbar_f\mathbf{N}_f\left[\widehat{f}(\eta;q_1^*)\right], \tag{30}$$

$$(1-q_1^*)\mathbf{L}_\theta\left[\widehat{\theta}(\eta;q_1^*)-\theta_0(\eta)\right]= q_1^*\hbar_\theta\mathbf{N}_\theta\left[\widehat{f}(\eta;q_1^*),\widehat{\theta}(\eta;q_1^*),\widehat{g}(\eta;q_1^*)\right], \tag{31}$$

$$(1-q_1^*)\mathbf{L}_g\left[\widehat{g}(\eta;q_1^*)-g_0(\eta)\right]= q_1^*\hbar_g\mathbf{N}_g\left[\widehat{f}(\eta;q_1^*),\widehat{\theta}(\eta;q_1^*),\widehat{g}(\eta;q_1^*)\right], \tag{32}$$

$$M\widehat{\theta}'(0;q_1^*)+\Pr\left(\widehat{f}(0;q_1^*)+\alpha\frac{n-1}{n+1}\right)=0,$$
$$\widehat{f}'(0;q_1^*)=1,\ \widehat{f}'(\infty;q_1^*)=A,$$
$$\widehat{\theta}(0;q_1^*)=0,\ \widehat{\theta}(\infty;q_1^*)=1-S,$$
$$\widehat{g}'(0;q_1^*)=\sqrt{\frac{2}{n+1}}K_s\widehat{g}(0;q_1^*),\ \widehat{g}(\infty;q_1^*)=1. \tag{33}$$

$$\mathbf{N}_f\left[\widehat{f}(\eta,q_1^*)\right]=\frac{\partial^3\widehat{f}(\eta,q_1^*)}{\partial\eta^3}+\frac{\varepsilon}{1+\varepsilon}\widehat{f}(\eta,q_1^*)\frac{\partial^2\widehat{f}(\eta,q_1^*)}{\partial\eta^2} -\frac{1+n}{1+\varepsilon}\delta^*\left(\frac{\partial^2\widehat{f}(\eta,q_1^*)}{\partial\eta^2}\right)^2\frac{\partial^3\widehat{f}(\eta,q_1^*)}{\partial\eta^3}+\frac{2n}{n+1}\frac{\varepsilon}{1+\varepsilon}A^2 -\frac{2n}{n+1}\frac{\varepsilon}{1+\varepsilon}\left(\frac{\partial\widehat{f}(\eta,q_1^*)}{\partial\eta}\right)^2+\frac{2Ha}{n+1}\frac{\varepsilon}{1+\varepsilon}A -\frac{2Ha}{n+1}\frac{\varepsilon}{1+\varepsilon}\frac{\partial\widehat{f}(\eta,q_1^*)}{\partial\eta}, \tag{34}$$

$$\mathbf{N}_\theta\left[\widehat{f}(\eta,q_1^*),\widehat{\theta}(\eta,q_1^*)\right]=\frac{\partial^2\widehat{\theta}(\eta,q_1^*)}{\partial\eta^2}-\frac{2\Pr}{1+n}\widehat{\theta}(\eta,q_1^*)\frac{\partial\widehat{f}(\eta,q_1^*)}{\partial\eta} -\frac{2\Pr S}{1+n}\frac{\partial\widehat{f}(\eta,q_1^*)}{\partial\eta}+\Pr\frac{\partial\widehat{\theta}(\eta,q_1^*)}{\partial\eta}\widehat{f}(\eta,q_1^*), \tag{35}$$

$$\mathbf{N}_g\left[\widehat{f}(\eta,q_1^*),\widehat{g}(\eta,q_1^*)\right]=\frac{\partial^2\widehat{g}(\eta,q_1^*)}{\partial\eta^2}-\frac{2ScK}{n+1}\widehat{g}(\eta,q_1^*) -\frac{2ScK}{n+1}\left(\widehat{g}(\eta,q_1^*)\right)^3+\frac{4ScK}{n+1}\left(\widehat{g}(\eta,q_1^*)\right)^2 +Sc\widehat{f}(\eta,q_1^*)\frac{\partial\widehat{g}(\eta,q_1^*)}{\partial\eta}, \tag{36}$$

here embedding parameter is represented by $q_1^*\in[0,1]$ and non-zero auxiliary parameters are denoted by h_f, $\hbar_\theta$ and $\hbar_g$.

3.2. Deformation of *m*th-order

$$\mathbf{L}_f\left[f_m(\eta)-\chi_m f_{m-1}(\eta)\right]=\hbar_f\mathbf{R}_m^f(\eta), \tag{37}$$

$$\mathbf{L}_\theta\left[\theta_m(\eta)-\chi_m\theta_{m-1}(\eta)\right]=\hbar_\theta\mathbf{R}_m^\theta(\eta), \tag{38}$$

$$\mathbf{L}_g\left[g_m(\eta)-\chi_m g_{m-1}(\eta)\right]=\hbar_g\mathbf{R}_m^g(\eta), \tag{39}$$

$$M\theta_m'(0)+\Pr\left(f_m(0)+\alpha\frac{n-1}{n+1}\right)=0,\ f_m'(0)=1,\ f_m'(\infty)=A,$$
$$\theta_m(0)=0,\ \theta_m(\infty)=1-S, \tag{40}$$

$$g_m'(0)=\sqrt{\frac{2}{n+1}}K_s g_m(0),\ g_m(\infty)=1, \tag{41}$$

$$\mathbf{R}_m^f(\eta)=f_{m-1}'''+\frac{\varepsilon}{1+\varepsilon}\sum_{k=0}^{m-1}f_{m-1-k}f_k''-\frac{1+n}{1+\varepsilon}\delta^*\sum_{k=0}^{m-1}f_{m-1-k}'''\sum_{l=0}^{k}f_{k-l}''f_l'' +\frac{2n}{n+1}\frac{\varepsilon}{1+\varepsilon}A^2(1-\chi_m)-\frac{2n}{n+1}\frac{\varepsilon}{1+\varepsilon}\sum_{k=0}^{m-1}f_{m-1-k}'f_k' +\frac{2Ha}{n+1}\frac{\varepsilon}{1+\varepsilon}A(1-\chi_m)-\frac{2Ha}{n+1}\frac{\varepsilon}{1+\varepsilon}f_{m-1}', \tag{42}$$

$$\mathbf{R}_m^\theta(\eta)=\theta_{m-1}''-\frac{2\Pr}{1+n}\sum_{k=0}^{m-1}(\theta_{m-1-k}f_k')-\frac{2\Pr S}{1+n}f_{m-1}' +\Pr\sum_{k=0}^{m-1}\theta_{m-1-k}'f_k, \tag{43}$$

$$\mathbf{R}_m^g(\xi)=g_{m-1}''-\frac{2ScK}{n+1}g_{m-1}-\frac{2ScK}{n+1}\sum_{k=0}^{m-1}g_{m-1-k}\sum_{l=0}^{k}g_{k-1}g_l +\frac{4ScK}{n+1}\sum_{k=0}^{m-1}g_{m-1-k}g_k+Sc\sum_{k=0}^{m-1}f_{m-1-k}g_k'. \tag{44}$$

$$\chi_m=\begin{cases}0, & m\le 1\\ 1, & m>1\end{cases}.$$

For $q_1^*=0$ and $q_1^*=1$ it follows,

$$\widehat{f}(\eta;0)=f_0(\eta),\ \widehat{f}(\eta;1)=f(\eta), \tag{45}$$

$$\widehat{\theta}(\eta;0)=\theta_0(\eta),\ \widehat{\theta}(\eta;1)=\theta(\eta), \tag{46}$$

$$\widehat{g}(\eta;0)=g_0(\eta),\ \widehat{g}(\eta;1)=g(\eta). \tag{47}$$

As q_1^* varies from 0 to 1 as a result $\widehat{f}(\eta;q_1^*)$, $\widehat{\theta}(\eta;q_1^*)$ and $\widehat{g}(\eta;q_1^*)$ change from the initial solutions $f_0(\eta)$, $\theta_0(\eta)$ and $g(\eta)$ to the final solutions $f(\eta)$, and $g(\eta)$ respectively. Following expressions are obtained for Taylor series at $q_1^*=1$,

$$f(\eta)=f_0(\eta)+\sum_{m=1}^{\infty}f_m(\eta), \tag{48}$$

$$\theta(\eta)=\theta_0(\eta)+\sum_{m=1}^{\infty}\theta_m(\eta), \tag{49}$$

$$g(\eta)=g_0(\eta)+\sum_{m=1}^{\infty}g_m(\eta). \tag{50}$$

General solutions (f_m, θ_m and g_m) in the form of special solutions (f_m^*, θ_m^* and g_m^*) are presented as:

$$f_m(\eta)=f_m^*(\eta)+E_1+E_2e^{\eta}+E_3e^{-\eta}, \tag{51}$$

$$\theta_m(\eta)=\theta_m^*(\eta)+E_4e^{\eta}+E_5e^{-\eta}, \tag{52}$$

$$g_m(\eta)=g_m^*(\eta)+E_6e^{\eta}+E_7e^{-\eta}. \tag{53}$$

Using boundary conditions we write

$$E_3 = E_4 = E_6 = 0,\ E_1 = -f_m^*(0) - \left.\frac{\partial f_m^*(\eta)}{\partial \eta}\right|_{\eta=0} - \frac{M}{\Pr}\left(\theta_m^*(0) + \left.\frac{\partial \theta_m^*(\eta)}{\partial \eta}\right|_{\eta=0}\right),$$
$$E_2 = \left.\frac{\partial f_m^*(\eta)}{\partial \eta}\right|_{\eta=0},\quad E_5 = -\theta_m^*(0), \tag{54}$$
$$E_7 = \frac{1}{\left(\sqrt{\frac{2}{n+1}}K_s + 1\right)}\left(\left.\frac{\partial g_m^*(\eta)}{\partial \eta}\right|_{\eta=0} - \sqrt{\frac{2}{n+1}}K_s g_m^*(0)\right).$$

4. Convergence Analysis

As suggested by Liao [38], homotopic procedures (*HAM*) are utilized to determine series solutions of the problem under consideration which is of highly nonlinear nature. It is well established argument about *HAM* that it provides sufficient convenience in adjusting and regulating region of convergence for series solution. In this regard, h curves are sketched to portray permissible ranges of $\hbar_f$, $\hbar_\theta$ and $\hbar_g$ (auxiliary parameters) i.e. $-1.4 \le \hbar_f \le -0.3$, $-1.2 \le \hbar_\theta \le -0.4$, $-1.35 \le \hbar_g \le -0.4$. With the help of numerical data Table 1 demonstrates the convergence of resultant series solutions. 7th order of approximation is noticed to be good enough for the solution to converge.

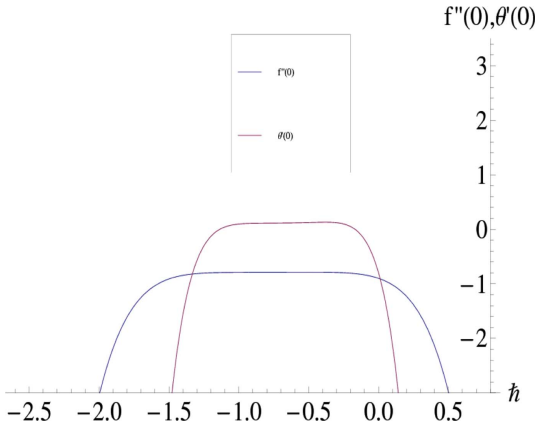

Fig. 2. (Color online) h-curve for $f(0)$ and $\theta(0)$.

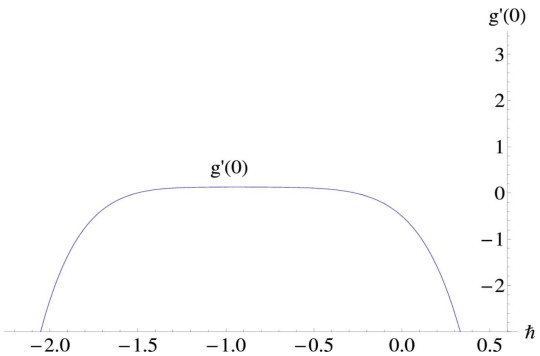

Fig. 3. (Color online) h-curve for $g(0)$.

Table 1. Convergence (HAM solutions) for $\varepsilon = \delta^* = M = K = 0.4$, $n = K_s = K = S = \alpha = \lambda = Ha = 0.2$, $A = 0.1$ and $\Pr = 1.2$.

Order of Approximation	$-f''(0)$	$\theta'(0)$	$g'(0)$
1	0.7695	0.1181	0.1382
3	0.7882	0.1813	0.1485
5	0.8889	0.1572	0.1949
7	0.8280	0.1416	0.1949
9	0.8280	0.1416	0.1949

The $\hbar$ – curves for $f(0)$, $\theta(0)$ and $g(0)$ when $\varepsilon = \delta^* = M = K = 0.4$, $n = K_s = K = S = \alpha = \lambda = Ha = 0.2$, $A = 0.1$ and $\Pr = 1.2$.

5. Discussion

This segment is devoted for analysis of different parameters with respect to velocity, thermal and concentration distributions. In Figs. 4-5 influence of fluid parameters ε and δ^* is portrayed for velocity profile $f'(\eta)$. Fig. 4 depicts declining attitude of $f'(\eta)$ for uplifted values of fluid parameter ε. Same is the case for momentum boundary layer thickness. We know $\varepsilon = \mu\beta C_1$, for increased ε it refers to enhancement in viscosity of fluid. Increment in viscosity ultimately reduces velocity field. Effect of fluid parameter δ^* upon the velocity field has been sketched in

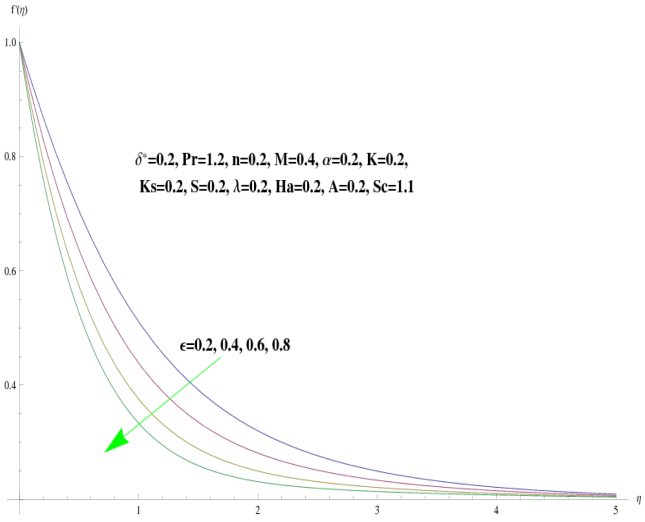

Fig. 4. (Color online) Display for ε over f'.

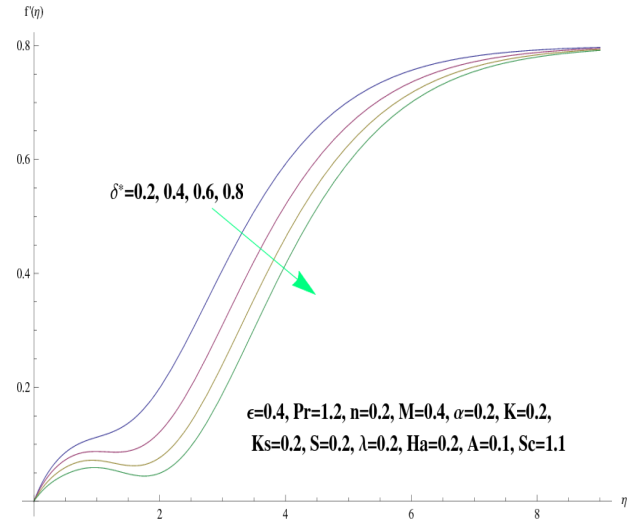

Fig. 5. (Color online) Display for δ^* over f'.

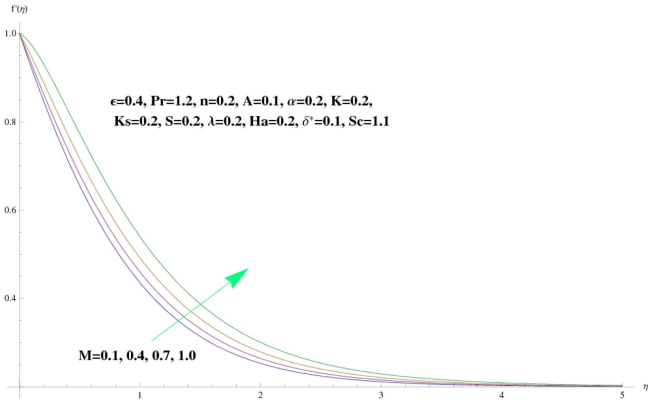

Fig. 6. (Color online) Display for M over f'.

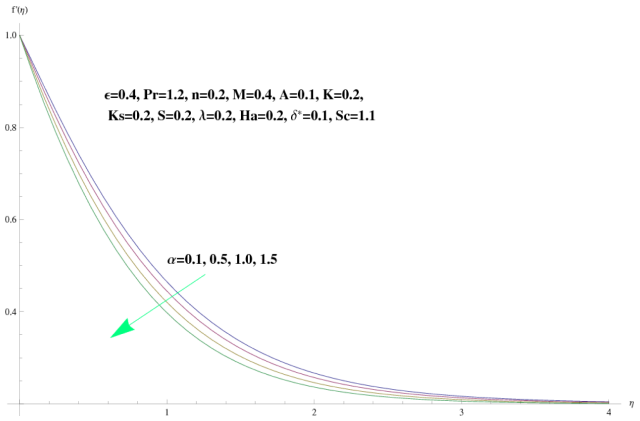

Fig. 7. (Color online) Display for α over f'.

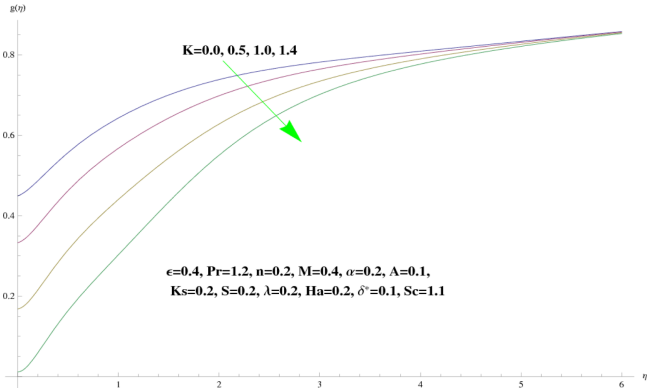

Fig. 8. (Color online) Display for K over g.

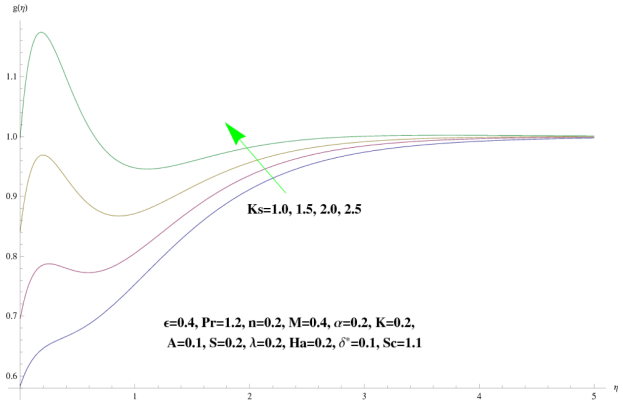

Fig. 9. (Color online) Display for K_s over g.

Fig. 5. It also shows the decrement in velocity field however momentum boundary layer thickness enhances in this case. Impact of melting parameter M on velocity field is established in Fig. 6. Evidently velocity field rises up for growing melting parameter and same is the case for momentum boundary layer thickness. It is justified by the reason as melting process gets intensified it gives rise to more convective flow which strengthens velocity field. The way wall thickness parameter α behaves for $f'(\eta)$ is revealed in Fig. 7. Larger values of α result in depreciated behavior of velocity profile $f'(\eta)$. Increment in α refers to strength of wall thickness due to which stretching behavior reduces and becomes the reason for weaker velocity. Fig. 8 interprets graphical behavior of K (homogeneous reaction parameter) for concentration field $g(\eta)$. Weak concentration field is obtained for higher intensity of K while boundary layer thickness gets boosted in this case. Influence of K_s (heterogeneous reaction parameter) on $g(\eta)$ is sketched in Fig. 9. Enhanced concentration profile is judged for developed intensity of K_s while declining behavior for concentration boundary layer thickness is observed. Fig. 10 describes features of Schmidt number Sc with respect to concentration field $g(\eta)$. Enhancement of concentration is observed for increasing Schmidt number Sc. Increment in Schmidt number refers to decreased mass diffusivity and it justifies the strength of the profile for concentration. While opposite

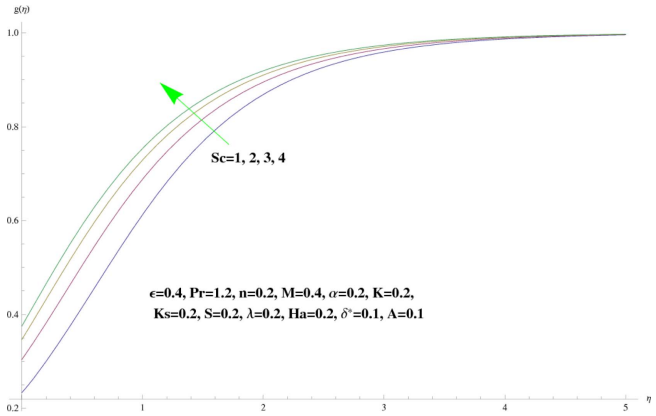

Fig. 10. (Color online) Display for *Sc* over *g*.

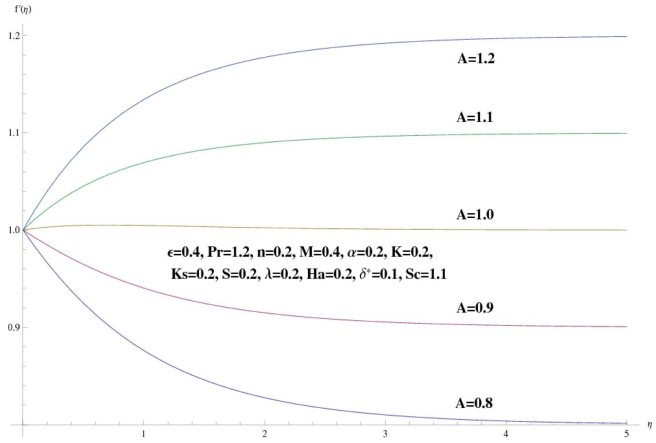

Fig. 11. (Color online) Display for A over f'.

behavior of boundary layer thickness is noted for solutal case. Fig. 11 shows influence of ratio velocity parameter A upon $f'(\eta)$. It is identified that velocity profile enhances as a result of larger values of A. It reveals an interesting behavior of momentum boundary layer thickness which grows up for $A < 1$ and it gets weaker for $A > 1$. It is worth mentioning no boundary layer occurs for the case $A = 1$. It is physically justified because for the case of $A = 1$ both wall and the fluid travel with identical velocities. Fig. 12 displays the impact of n (the power index) on $f'(\eta)$. Weaker velocity profile is depicted for higher power index n. While Fig. 13 show impact of melting parameter on thermal field $\theta(\eta)$. Depreciated behavior of temperature field is noted as a result of increase in M. For the case of strength of M, greater amount of heat gets shifted from heated fluid towards melting surface which ultimately lessens temperature of fluid. Fig. 14 interprets the analysis of λ on thermal field $\theta(\eta)$. Due to higher values of λ there is seen decrement in thermal field. It is physically endorsed as heat generation process enhances convective type of flow from hot fluid to melting

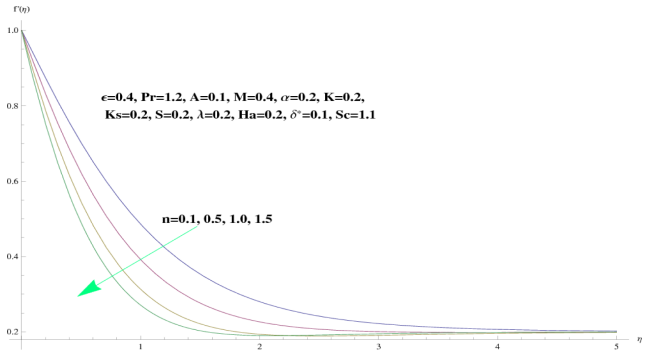

Fig. 12. (Color online) Display for n over f'.

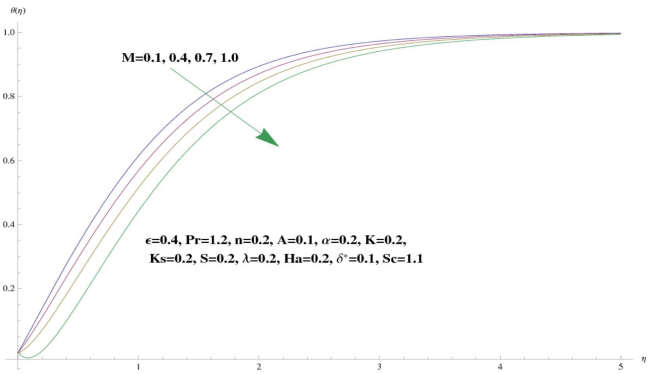

Fig. 13. (Color online) Display for M over θ.

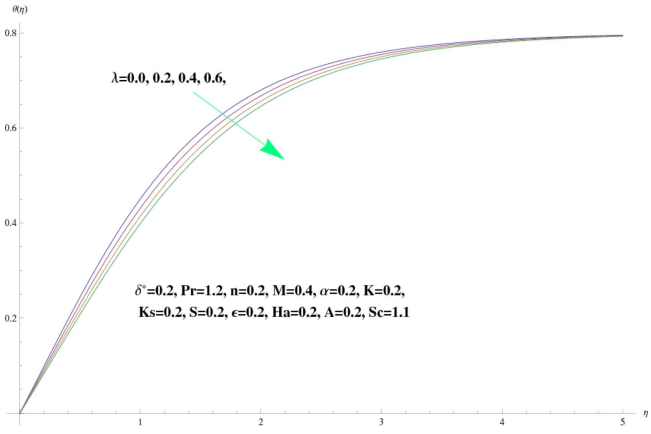

Fig. 14. (Color online) Display for λ over θ.

surface and ultimately temperature of fluid decreases. However thermal boundary layer thickness exhibits opposite behavior. Fig. 15 gives comprehension of Prandtl number Pr for thermal distribution $\theta(\eta)$. Clearly temperature rises as Prandtl number increases. Due to lower thermal diffusivity lesser heat transfers from fluid at high temperature to the cold surface and ultimately temperature of fluid remains high. On contrary to this thermal boundary layer thickness shows weaker attitude. Characteristics of Hartman number Ha and α for skin friction coefficient C_f are

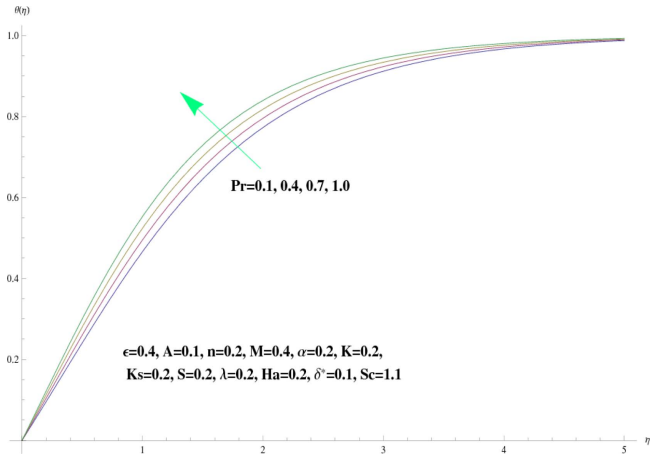

Fig. 15. (Color online) Display for Pr over θ.

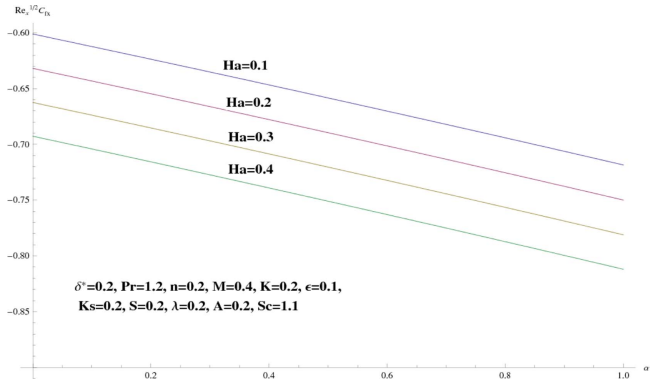

Fig. 16. (Color online) Display for Ha and α over C_f.

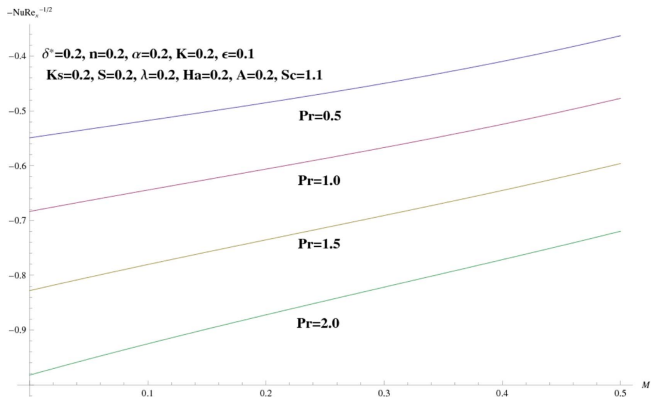

Fig. 17. (Color online) Display for Pr and M over Nu.

scrutinized in Fig. 16. C_f depreciates both for wall thickness parameter α as well as Hartman number Ha. Demonstration regarding effect of M and Pr on Nusselt number is given in Fig. 17. Nusselt number shows recessive outcome for higher melting parameter$M$ however progressive behavior is noted for Prandtl number Pr. Comparative results reveal good agreement (see Table 2) for different values of $f''(0)$ with already published data in the limiting case.

Table 2. Comparative data of $f''(0)$ with previous published results for A = 0.1, 0.2, 0.5, 0.7, 0.9 when $\varepsilon = 0$, $\delta^* = 0$, $Ha = 0$, $n = 1$.

A	Pop *et al.* [34]	Mahapatra and Gupta [35]	Sharma and Singh [36]	Present results
0.1	–0.9694	–0.9694	–0.969386	–0.969391
0.2	–0.9181	–0.9181	–0.918106	–0.918119
0.5	–0.6673	–0.6673	–0.667263	–0.667270
0.7				–0.433462
0.9				–0.154581

6. Closing Remarks

Aspects of heat transfer via melting process with chemical species are studied in thermally stratified MHD flow of Eyring-Powell fluid towards a sheet of varying thickness. Concluding key features are summarized as follows:

1. Velocity field declines as a result of increment in fluid parameters ε as well as δ^*.
2. Increment in Schmidt number enhances concentration profile.
3. Concentration of reactants exhibit recessive behavior as a result of boosted values of K.
4. Growth of K_s results in intensified field for concentration.
5. Thermal field drops with growth of heat generation/absorption parameter.
6. Skin friction gets weaker for uplifted wall thickness parameter.
7. Gradual decline in thermal field is noticed for increased melting parameter.

References

[1] J. H. Merkin, Math. Comp. Model **24**, 125 (1996).
[2] T. Yasmeen, T. Hayat, M. I. Khan, M. Imtiaz, and A. Alsaedi, J. Mol. Liq. **223**, 1000 (2016).
[3] N. Sandeep, C. Sulochana, and A. I. Lare, Int. J. Engg. Res. in Afr. **20**, 93 (2016).
[4] M. I. Khan, M. Waqas, T. Hayat, and A. Alsaedi, Int. J. Coll. Int. Sci. **498**, 85 (2017).
[5] T. Hayat, M. Farooq, and A. Alsaedi, AIP Adv. **5**, 027130 (2015).
[6] Q. Lu, J. Pan, W. Yang, A. Tang, S. Bani, and X. Shao, Int. J. Hyd. Energy **42**, 5390 (2017).
[7] S. K. Adegbie, O. K. Koriko, and I. L. Animasaun, J. Nig. Math., Soc. **35**, 34 (2016).

[8] M. A. A. Mahmoud and S. E. Waheed, App. Math. Mech. **35**, 979 (2014).
[9] M. S. Abel and J. Sanamani, IOSR J. Math. **11**, 91 (2015).
[10] F. Mabood and K. Das, Eur. Phys. J. Plus **3**, 131 (2016).
[11] M. Farooq, M. Javed, M. I. Khan, A. Anjum, and T. Hayat, Res. in Phys. **7**, 2296 (2017).
[12] M. Javed, M. Farooq, S. Ahmad, and Aisha Anjum, J. Cent. S. Uni. **25**, 2701 (2018).
[13] M. Usman, F. A. Soomro, R. U. Haq, W. Wang, and O. Defterli, Int. J. Heat Mass Tran. **122**, 1255 (2018).
[14] F. A. Soomro, R. U. Haq, Q. M. Al-Mdallal, and Q. Zhang, Res. in Phys. **8**, 404 (2018).
[15] F. U. Rehman, S. Nadeem, H. U. Rehman, and R. U. Haq, Res. in Phys. **8**, 316 (2018).
[16] M. Usman, T. Zubair, M. Hamid, R. U. Haq, and W. Wang, Phys. of Fluids **30**, 023104 (2018).
[17] M. Usman, R. U. Haq, M. Hamid, and W. Wang, Int. J. Mol. Liq. **249**, 856 (2018).
[18] S. S. Ghadikolaei, K. Hosseinzadeh, and D. D. Ganji, Powd. Tech. **338**, 425 (2018).
[19] S. S. Ghadikolaei, K. Hosseinzadeh, D. D. Ganji, and B. Jafari, Case St. Ther. Engg. **12**, 176 (2018).
[20] A. Shojaei, A. J. Amiri, S. S. Ardahaie, K. Hosseinzadeh, and D. D. Ganji, Case St. Ther. Engg. **13**, 100384 (2019).
[21] A. S. Dogonchi, M. Hatami, K. Hosseinzadeh, and G. Domairry, Powd. Tech. **278**, 248 (2015).
[22] S. S. Ghadikolaei, K. Hosseinzadeh, M. Yassari, H. Sadeghi, and D. D. Ganji, Ther. Sci. Engg. Prog. **5**, 309 (2018).
[23] S. S. Ardahaie, A. J. Amiri, A. Amouei, K. Hosseinzadeh, and D. D. Ganji, Info. Med. Unlock. **10**, 71 (2018).
[24] K. Hosseinzadeh, A. J. Amiri, S. S. Ardahaie, and D. D. Ganji, Case St. Ther. Engg. **10**, 595 (2017).
[25] S. A. Atouei, K. Hosseinzadeh, M. Hatami, S. E. Ghasemi, S. A. R. Sahebi, and D. D. Ganji, App. Ther. Engg. **89**, 299 (2015).
[26] R. E. Powell and H. Eyring, Nature **154**, 427 (1944).
[27] M. A. Megahed, Zeits. für Naturfor. A. **70**, 163 (2015).
[28] M. Jalil, S. Asghar, and S. M. Imran, Int. J. of Heat and Mass Tran. **65**, 73 (2013).
[29] A. Ara, N. A. Khan, H. Khan, and F. Sultan, Ain Shams Engg. J. **5**, 1337 (2014).
[30] T. Hayat, S. Ali, M. A. Farooq, and A. Alsaedi, PLoS One **10**, 1 (2015).
[31] M. Gholinia, K. Hosseinzadeh, H. Mehrzadi, D. D. Ganji, and A. A. Ranjbar, Case St. Ther. Engg. **13**, 100356 (2019).
[32] J. Rahimi, D. D. Ganji, M. Khaki, and K. Hosseinzadeh, Alex. Engg. J. **56**, 621 (2017).
[33] S. S. Ghadikolaei, K. Hosseinzadeh, and D. D. Ganji, Case St. Ther. Engg. **10**, 579 (2017).
[34] S. Pop, T. Grosan, and I. Pop, Techn. Mech. **25**, 100 (2004).
[35] T. R. Mahapatra and A. Gupta, Heat Mass Trans. **38**, 517 (2002).
[36] P. Sharma and G. Singh, J. Appl. Fluid Mech. **2**, 13 (2009).
[37] L. Shijun, App. Math and Mech. **10**, 957 (1998).
[38] S. J. Liao, Homotopy analysis method in non-linear differential equations (Springer and Higher Education Press, Heidelberg, 2012).
[39] S. Abbasbandy, M. S. Hashemi, and I. Hashim, Quaestiones Mathematicae **36**, 93 (2013).
[40] M. Turkyilmazoglu, Commun. Nonlinear Sci. Numer. Simulat. **17**, 4097 (2012).
[41] M. Khan and W. A. Khan, J. Mol. Liq. **221**, 651 (2016).
[42] T. Hayat and M. Sajid, Phys. Lett. A **361**, 316 (2007).
[43] J. Zhu, D. Yang, L. Zheng, and X. Zhang, Appl. Math. Letters **52**, 183 (2016).
[44] T. Hayat, M. Farooq, and A. Alsaedi, Int. J. Num. Meth. Heat Fluid Flow **25**, 724 (2015).
[45] H. Hassan and M. M. Rashidi, Int. J. Num. Meth. Heat Fluid Flow **24**, 419 (2014).
[46] T. Hayat, S. Ali, M. Awais, and M. S. Alhuthali, App. Math. and Mech. (English Edition) **36**, 61 (2015).